Engineering opposite electronic polarization of singlet and triplet states increases the yield of high-energy photoproducts

Nicholas F. Polizzi[a], Ting Jiang[b], David N. Beratan[a,b,c,1], and Michael J. Therien[b,1]

[a]Department of Biochemistry, Duke University, Durham, NC 27710; [b]Department of Chemistry, Duke University, Durham, NC 27708; and [c]Department of Physics, Duke University, Durham, NC 27708

Edited by Richard Eisenberg, University of Rochester, Rochester, NY, and approved May 15, 2019 (received for review January 30, 2019)

Efficient photosynthetic energy conversion requires quantitative, light-driven formation of high-energy, charge-separated states. However, energies of high-lying excited states are rarely extracted, in part because the congested density of states in the excited-state manifold leads to rapid deactivation. Conventional photosystem designs promote electron transfer (ET) by polarizing excited donor electron density toward the acceptor ("one-way" ET), a form of positive design. Curiously, negative design strategies that explicitly avoid unwanted side reactions have been underexplored. We report here that electronic polarization of a molecular chromophore can be used as both a positive and negative design element in a light-driven reaction. Intriguingly, prudent engineering of polarized excited states can steer a "U-turn" ET—where the excited electron density of the donor is initially pushed away from the acceptor—to outcompete a conventional one-way ET scheme. We directly compare one-way vs. U-turn ET strategies via a linked donor–acceptor (DA) assembly in which selective optical excitation produces donor excited states polarized either toward or away from the acceptor. Ultrafast spectroscopy of DA pinpoints the importance of realizing donor singlet and triplet excited states that have opposite electronic polarizations to shut down intersystem crossing. These results demonstrate that oppositely polarized electronically excited states can be employed to steer photoexcited states toward useful, high-energy products by routing these excited states away from states that are photosynthetic dead ends.

excited-state dynamics | electron transfer | photoenergy conversion | polarization | intersystem crossing

Photosynthetic energy transduction is limited by the energy of the initially formed excited state, which typically relaxes on an ultrafast timescale, releasing a significant portion of energy of the absorbed photon as heat. Indeed, rapid internal conversion between higher and lowest-lying singlet excited states ($S_n \rightarrow S_1$) is responsible for a significant drop in the thermodynamic efficiency of natural photosystems (1), as is ultrafast intersystem crossing to lower-energy triplet states in their artificial counterparts (2). The ability to control the fate of the initially prepared excited state on this ultrafast timescale is notoriously challenging, in part because many close-lying vibronic excited states encumber the engineering of large energy gaps to control dynamics. However, transition rates between states are also governed by coupling interactions at surface crossings, ultimately proportional to wave function overlap (3). Here, we test the idea that electronic polarization of electronically excited states can control excited-state reaction trajectories on the ultrafast timescale, by tuning wave function overlap between competing states.

Excited-state polarization of an electron donor has classically been engineered in molecular donor–bridge–acceptor systems to promote an electron transfer (ET) reaction by pushing electron density of the donor toward an acceptor upon absorption of the incident photon (4, 5). This intuitive, one-way ET scheme is a positive design strategy: It promotes the formation of the final, charge-separated state by directly influencing the transition rate via an enhanced electronic coupling interaction between the initial and final state. However, when the density of states is congested, states competing with the target state need to be explicitly avoided. We wondered if electronic polarization could also be employed as a negative design strategy. Intriguingly, we indeed find that engineering of oppositely polarized excited states can promote population of the charge-separated state, even if the initial excited-state electron density is pushed away from the acceptor (U-turn ET). This work illustrates a means to purposefully traverse a dense excited-state singlet and triplet manifold on the ultrafast timescale: we show that antiparallel electronic polarizations of singlets and triplets can be engineered in the same chromophore to maximally preserve the energy of the incident photon in a final charge-separated state, critical for efficient artificial photosystems.

Results and Discussion

To explore excited-state electronic polarization as a positive and negative design strategy, we needed a model electron donor (D) possessing electronically excited states with substantial yet oppositely oriented polarizations. The existence of oppositely polarized charge-transfer (CT) excited states within the same chromophore is unusual. In this regard, the supermolecule RuPZn is exemplary (Fig. 1 and *SI Appendix*, Fig. S1) (6–8). The RuPZn chromophore consists of ruthenium(II)polypyridyl (Ru) and (porphinato)zinc(II) (PZn) units connected via an ethyne bridge. This connectivity aligns the Ru and PZn transition dipoles in a head-to-tail arrangement, enforcing extensive excited-state interpigment electronic communication that gives rise to

Significance

All known natural reaction centers employ high-energy singlet states as electron donors, but artificial photosystems struggle to overcome energy losses associated with lower-energy triplet-state formation, which critically limits solar energy conversion efficiency. Our results illustrate a design principle—seemingly at work in the photosynthetic reaction center of *Rhodobacter sphaeroides*—that employs oppositely polarized singlet and triplet excited states to avert intersystem crossing and dramatically increase the yield of high-energy photoproducts, critical for enhanced efficiency solar cells.

Author contributions: N.F.P., T.J., and M.J.T. designed research; N.F.P. and T.J. performed research; T.J. contributed new reagents/analytic tools; N.F.P., T.J., D.N.B., and M.J.T. analyzed data; and N.F.P., T.J., D.N.B., and M.J.T. wrote the paper.

The authors declare no conflict of interest.

This article is a PNAS Direct Submission.

See Commentary on page 14398.

[1]To whom correspondence may be addressed. Email: david.beratan@duke.edu or michael.therien@duke.edu.

This article contains supporting information online at www.pnas.org/lookup/suppl/doi:10.1073/pnas.1901752116/-/DCSupplemental.

Published online June 10, 2019.

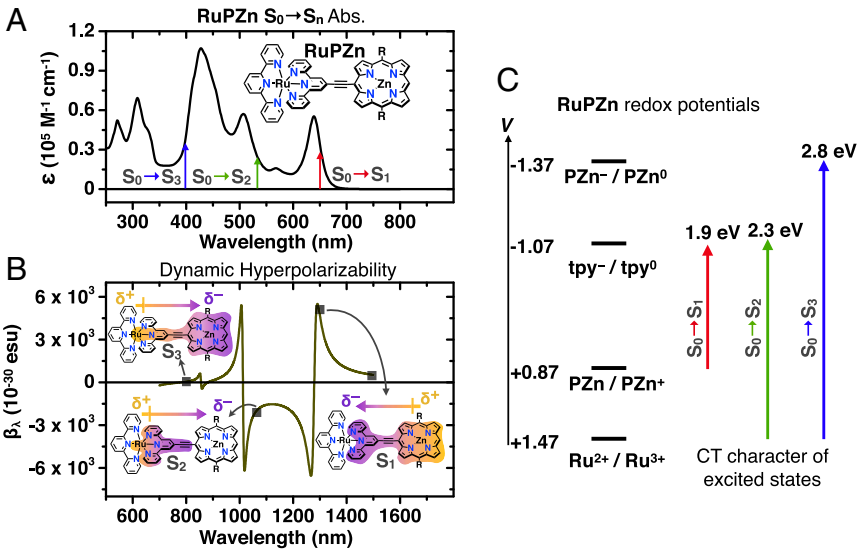

Fig. 1. The excited states of RuPZn have oppositely oriented electric dipole moments. (*A*) The electronic absorption spectrum of RuPZn displays distinct absorption manifolds into S_1 (red), S_2 (green), and S_3 (blue) excited states. Arrows demark the excitation (pump) wavelengths of RuPZn used in the pump–probe experiments of this report, which are also the two-photon-resonant wavelengths of the dynamic hyperpolarizability (β_λ) experiments (boxes) in *B*. (*B*) β_λ-spectrum (gold) of RuPZn determined from experimentally measured values (boxes) (6, 11, 12). See *SI Appendix* for more details. (*C*) One-electron oxidation and reduction potentials (vs. standard calomel electrode) of RuPZn in acetonitrile solvent. Colored arrows show that the one-electron oxidations and reductions track with the ground- to excited-state energies. These one-electron transitions qualitatively describe the CT character of the corresponding excited states, as well as the electronic polarizations described in *B*.

significant CT character in the lowest three singlet excited states (S_1, S_2, and S_3) (6–11). The unusual frequency dispersion of the RuPZn molecular hyperpolarizability, highlighted in part by the large dynamic hyperpolarizability (β_λ) at 1,300-nm incident irradiation (Fig. 1*B*), and the small β_λ at 800 nm, indicate that S_1 has an electric dipole moment that is antiparallel to that of S_2 and S_3 (6, 9–12). S_2 and S_3 feature electron density pushed from Ru toward PZn, while S_1 features electron density oppositely polarized from PZn toward Ru (Fig. 1*B*). Two- and three-level models for β_λ (6, 9–12), along with energetic considerations of the CT transitions (6), support these assignments (*SI Appendix*). Indeed, the dipole magnitudes of S_1, S_2, and S_3 are substantial, calculated to span a 13–43-D range (12). The corresponding triplet manifold of RuPZn is similarly polarized, belying its long (44-μs) triplet-state lifetime, due to attenuated Franck–Condon overlap with the ground state (7). Although the excited states of RuPZn are highly delocalized and described by extensive configuration interaction (6, 9–12), an appealing picture that rationalizes these unusually strong singlet and triplet electronic polarizations can be painted by comparing the one-electron redox potentials of RuPZn to the energy of its excited states (Fig. 1*C*). For instance, a red photon possesses enough energy to formally oxidize the PZn unit and reduce the terpyridyl (tpy) unit, which is consistent with the CT character of S_1; a blue photon possesses enough energy to formally oxidize Ru^{2+} and reduce the PZn unit, consistent with the CT character of S_3.

In the context of ET, selective optical excitation of a RuPZn electron donor (D → ^{1}D*) with blue or red light generates excited singlet states that are oppositely polarized: Such states may be used to trigger one-way or U-turn ET reactions (Fig. 2), which can be subsequently tracked via transient absorption pump–probe experiments. An ET reaction must occur on a timescale similar to that of the electronically excited-state lifetime, which is typically short-lived. For example, to employ both S_3 and S_1 states of RuPZn as distinct donor states, ET from S_3 must occur in less than 1 ps because S_3-to-S_1 internal conversion occurs in 0.7 ps (*vide infra*). We therefore directly linked a naphthalene diimide (NDI) electron acceptor to the PZn unit of RuPZn (Fig. 2 and *SI Appendix*). The steric hindrance between the PZn unit and NDI carbonyl groups imparts a large torsional angle between the planes of PZn and NDI (13, 14); consequently, the DA molecule RuPZn–NDI retains the chromophoric properties inherent to RuPZn (*SI Appendix*, Fig. S2). Such intimately linked donor–acceptor (DA) complexes are known to have mean-square

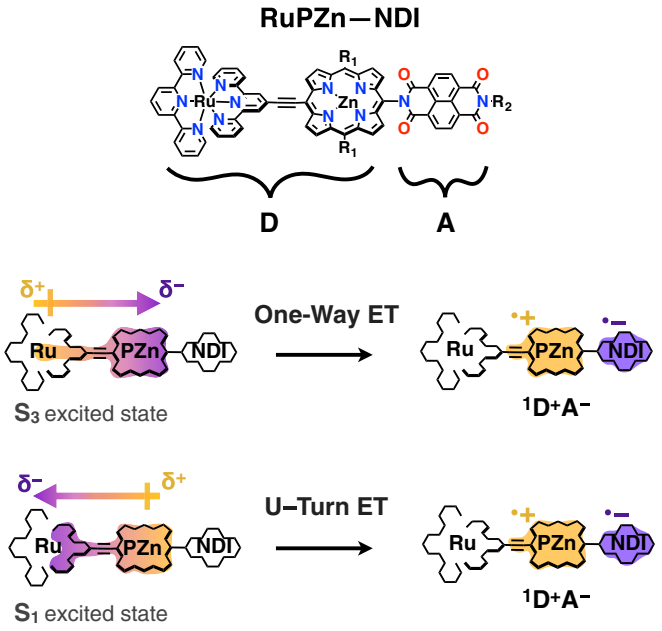

Fig. 2. Photoinduced ET schemes. The molecular structure of the DA molecule, RuPZn–NDI is shown, along with one-way, and U-turn ET schemes. One-way or U-turn ET events are phototriggered by excitation of the donor (D) chromophore (RuPZn) into its S_3 or S_1 singlet excited states, respectively. Structures of ancillary groups R_1 and R_2 are shown in *SI Appendix*, Scheme S1.

electronic couplings on the scale of tens of meV (13). DA couplings on this scale place their ET reactions well within the adiabatic regime, without causing sufficient ground-state mixing such that the D- and A units would lose their individual spectroscopic identities.

The pump–probe transient dynamics of RuPZn–NDI following electronic excitation into its oppositely polarized, RuPZn-localized singlet states (^{1}D*A) show that U-turn ET produces a substantially higher yield of the high-energy, singlet charge-separated state (^{1}D$^+$A$^-$) than does one-way ET (Fig. 3). A narrowband, blue pump pulse (400 ± 5 nm) prepares a one-way ET reaction from S_3 (Fig. 3*A*), whereas a red pump (650 ± 5 nm) poises a U-turn ET event from S_1 (Fig. 3*C*). These pump pulses partially depopulate the electronic ground state of RuPZn–NDI, observed as negative signal (ground-state bleach); the formation of transient excited states is revealed by positive signal (excited-state absorption). Excited-state evolution is monitored via the rise and decay of distinct spectral features, as a function of pump–probe time delay.

One-way ET (Fig. 3 *A* and *B*) from S_3 is outcompeted by intersystem crossing to the RuPZn-localized triplet state (^{3}D*A, cyan spectrum), which has the spectroscopic hallmark of a broad, high-oscillator-strength, near-IR absorption (Fig. 4*B* and *SI Appendix*, Fig. S3) (7, 8, 10). Ultrafast formation of ^{3}D*A from ^{1}D*A leads to slow, thermodynamically viable triplet ET (orange arrows), producing the lower-energy triplet charge-separated state (^{3}D$^+$A$^-$, orange spectrum), which has spectral signatures analogous to ^{1}D$^+$A$^-$ that include prominent 480- and 610-nm absorption bands associated with A$^-$ (15). At 1-ps time delay (black spectrum), the large ratio of the 930-nm signal (predominantly ^{3}D*A) to the 480-nm signal (predominantly ^{1}D$^+$A$^-$) indicates that ultrafast intersystem crossing cripples one-way ET to ^{1}D$^+$A$^-$. Indeed, the rise of the 480-nm absorption on a 130-ps timescale (Fig. 3*B* and *SI Appendix*, Figs. S3–S5), which occurs concomitantly with the loss of the 930-nm absorption, shows a large yield of ^{3}D$^+$A$^-$ instead. These ^{3}D$^+$A$^-$ states, produced in high yield, decay through charge recombination with a time constant of 30 ns (*SI Appendix*, Fig. S6).

Conversely, photopreparation of S_1, which pushes electron density of ^{1}D* away from A, predominantly achieves ultrafast ET to ^{1}D$^+$A$^-$ (Fig. 3*C*). The spectral signatures of ^{1}D$^+$A$^-$ overwhelm the 1-ps transient spectrum (black); a weak transient spectrum at 10.5-ps time delay (cyan) indicates extremely attenuated ^{3}D*A formation, from which ^{3}D$^+$A$^-$ is formed (orange spectrum). The fast rise and decay of ^{1}D$^+$A$^-$, observed at the 480-nm signature of A$^-$ during time delays less than 10 ps, overshadows the slower (>100 ps) rise of A$^-$ associated with ^{3}D$^+$A$^-$ (Fig. 3*D*, purple trace). Upon $S_0 \rightarrow S_1$ excitation, most of the excited ^{1}D*A population is funneled away from ^{3}D*A and into ^{1}D$^+$A$^-$, shown also by the severely diminished 930-nm signature of ^{3}D*A at time delays greater than 10 ps (Fig. 3*D*, gold trace), relative to that found after $S_0 \rightarrow S_3$ excitation (Fig. 3*B*, gold trace). Indeed, the ratio of the quantum yields of formation of ^{1}D$^+$A$^-$ relative to ^{3}D$^+$A$^-$ is 20:1 via U-turn ET from S_1, and only 1:2 via one-way ET from S_3. These data indicate that excited-state polarization of the asymmetrical supermolecular RuPZn chromophore is key to the vastly disparate ET yields shown here (Fig. 3; see also control experiments described in *SI Appendix*, Fig. S7).

The pivotal electronic factor governing singlet ET efficiency in RuPZn–NDI is spatial wave function overlap between the singlet and triplet excited states of D (^{1}D*A and ^{3}D*A). In the isolated RuPZn molecule, the ^{1}D* states undergo intersystem crossing to a highly polarized, metal-to-ligand CT triplet state (^{3}D*) in high yield (7, 8). While high yields of triplet-state formation are a general and characteristic feature of metal-polypyridyl chromophores, the highly polarized nature of the triplet ^{3}D* state is a unique characteristic of the asymmetrical RuPZn supermolecule. Pump–probe transient absorption data indicate that the intersystem crossing timescale of RuPZn is subpicosecond from S_3 (Fig. 4*B* and *SI Appendix*, Fig. S1*D*) and

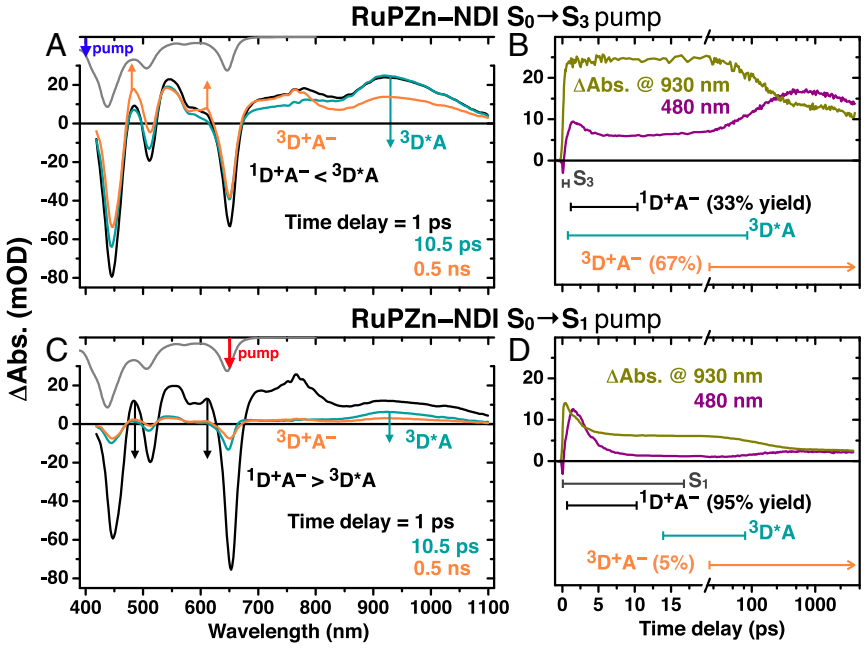

Fig. 3. Excited-state evolution of RuPZn–NDI upon triggering one-way and U-turn ET events. (*A* and *C*) Pump–probe transient absorption difference (ΔAbs.) spectra of RuPZn–NDI in acetonitrile solvent following $S_0 \rightarrow S_3$ and $S_0 \rightarrow S_1$ excitation, respectively, at three time delays; color-coded labels denote the state that makes the dominant contribution to the transient spectrum. $S_0 \rightarrow S_3$ excitation poises a one-way ET event, while $S_0 \rightarrow S_1$ excitation poises a U-turn ET event. Arrows point in the direction of spectral evolution. The inverted, scaled electronic absorption spectrum of RuPZn–NDI is shown at the top of *A* and *C*. (*B* and *D, Upper*) Two kinetic traces of the pump–probe data in *A* and *C*. Gold traces primarily track the RuPZn-localized triplet state (^{3}D*A); purple traces primarily track A$^-$ absorption of the singlet and triplet charge-separated states (^{1}D$^+$A$^-$ and ^{3}D$^+$A$^-$, respectively). (*B* and *D*, *Lower*) Lengths of the horizontal bars denote the time windows where these states are populated. Time delay is a log scale after the axis break.

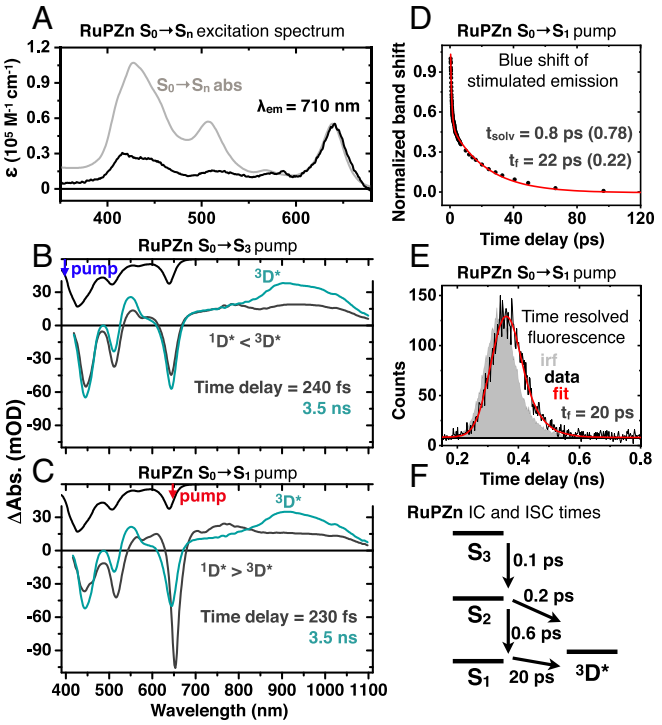

Fig. 4. Intersystem crossing is controlled by excited-state polarization. (*A*) Excitation spectrum (black) of RuPZn in acetonitrile solvent, monitoring ^{1}D* fluorescence at 710 nm. The spectrum is scaled such that signal at 638 nm is equal in magnitude to the absorbance band (gray). (*B* and *C*) Pump–probe transient absorption difference (ΔAbs.) spectra of RuPZn in acetonitrile solvent following $S_0 \rightarrow S_3$ and $S_0 \rightarrow S_1$ excitation, respectively, at two time delays, with dominant character indicated by the color-coded state labels. The inverted, scaled electronic absorption spectrum of RuPZn is shown at the top of *B* and *C*. (*D*) $S_0 \rightarrow S_1$ bleaching band minimum shift of RuPZn in acetonitrile solvent, as a function of pump–probe time delay. The blue shift of this band tracks S_1 state solvation (t_s) and intersystem crossing (t_f) timescales. Time constants are from a biexponential fit. Numbers in parentheses are the relative amplitudes. (*E*) Time-resolved fluorescence of RuPZn, integrated over the 660–760-nm window; t_f is the emission lifetime. (*F*) Kinetics of intersystem crossing (ISC) and internal conversion (IC), derived from time-resolved and steady-state data in *A*–*E*.

~20 ps from S_1 (Fig. 4 *C*–*E* and *SI Appendix*, Fig. S1*D*), consistent with S_3 and ^{3}D* possessing similar Ru-to-PZn CT character. The identical polarizations of the S_3 and ^{3}D* electronic states ensure that the nuclear potential energy surfaces are strongly split in their crossing region (Fig. 5*C*), in contrast to the potential surfaces corresponding to the oppositely polarized S_1 and ^{3}D* states (Fig. 5*D*). By pushing electron density toward the acceptor, one-way ET from S_3 of RuPZn–NDI is intercepted by intersystem crossing to a similarly polarized ^{3}D*A. On the other hand, the opposite dipole moments of S_1 and ^{3}D*A attenuate their spatial wave function overlap, dramatically slowing the intersystem crossing rate. Consequently, U-turn ET becomes not only viable from a longer-lived S_1 but also maximizes the yield of ^{1}D$^+$A$^-$ (Figs. 5 and 6).

Photoinduced charge separation from both the S_1 and S_3 states occurs on the ultrafast timescale, congruent with these processes being adiabatic (Fig. 5 *C* and *D*). In the adiabatic regime, the probability of transitioning from the initial to final state is unity, and the rate does not depend on the electronic coupling. Indeed, in this regime, U-turn ET in RuPZn–NDI (0.8 ps) is slightly faster than one-way ET (1.1 ps), despite what would otherwise be considered a stronger electronic coupling for the latter (Fig. 6). Moreover, these ultrafast CS timescales indicate the excited vibrational state distribution is not thermalized. As such, the ET rate cannot be characterized using the high-temperature Marcus expression for the Franck–Condon factor (that would otherwise link an activation free energy to driving force and reorganization energy) (16). Nevertheless, we expect U-turn ET to elicit a larger reorganization energy than one-way ET, which may impact Franck–Condon factors associated with the transition. As solvent plays a large role in outer-sphere ET reactions, we expect the role of reorganization energy to become more pronounced with increasing solvent polarity.

Intuitively, engineering electronic-state wave functions to "look alike" has long been a design goal to maximize the transition rate between states (3); however, the success of U-turn ET shown here emphasizes a consideration of equal importance for engineering state wave functions to "look different," to minimize access to undesirable reaction pathways. The ^{3}D*A states of RuPZn–NDI eventually transition to the lower-energy triplet charge-separated state ^{3}D$^+$A$^-$ (Figs. 3 and 5). It is interesting to note that for some organisms that exploit light-driven ET reactions—such as the purple bacterium *Rhodobacter sphaeroides*—triplet ET is not thermodynamically viable (17, 18); in this case, the formation of long-lived ^{3}D*A in such organisms is not only energetically wasteful, it is physically harmful to the organism if the excited-state energy is not dissipated as heat.

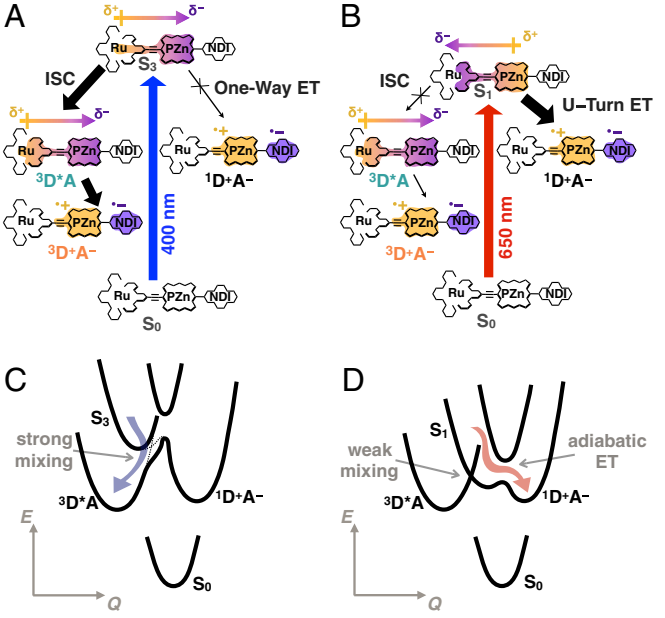

Fig. 5. Electronic polarization determines the fate of the initially prepared excited state. (*A*) Light absorption that polarizes donor (RuPZn) electron density toward the acceptor (NDI) in a one-way ET mechanism results in a low yield of singlet ET products (^{1}D$^+$A$^-$), due to fast intersystem crossing (ISC) to similarly polarized, donor-localized triplet state (^{3}D*A). Slow triplet ET from ^{3}D*A of RuPZn–NDI then produces triplet ET products (^{3}D$^+$A$^-$). (*B*) In U-turn ET, donor (D) electron density is pushed away from the acceptor (A), which slows ISC to ^{3}D*A, which is characterized by an oppositely oriented electric dipole moment. U-turn ET thereby maximizes the yield of ^{1}D$^+$A$^-$. (S_0, ground electronic state; S_1 and S_3, first and third singlet excited states, respectively. Note that ^{1}D$^+$A$^-$ corresponds to the relaxed, charge-separated singlet state.) (*C* and *D*) Qualitative potential energy diagrams describing one-way (*C*, $S_0 \rightarrow S_3$ excitation) and U-turn (*D*, $S_0 \rightarrow S_1$ excitation) ET schemes in RuPZn–NDI, where *E* denotes relative state energies and *Q* a nuclear polarization coordinate. Both S_1 and S_3 manifest adiabatic curve crossings with ^{1}D$^+$A$^-$. Identical S_3 and ^{3}D*A electronic polarizations give rise to strong mixing between these states and manifest ultrafast intersystem crossing. As S_1 and ^{3}D*A are oppositely polarized, these states are weakly mixed. Hence, S_1 excitation drives larger charge-separated product yields because ISC is suppressed.

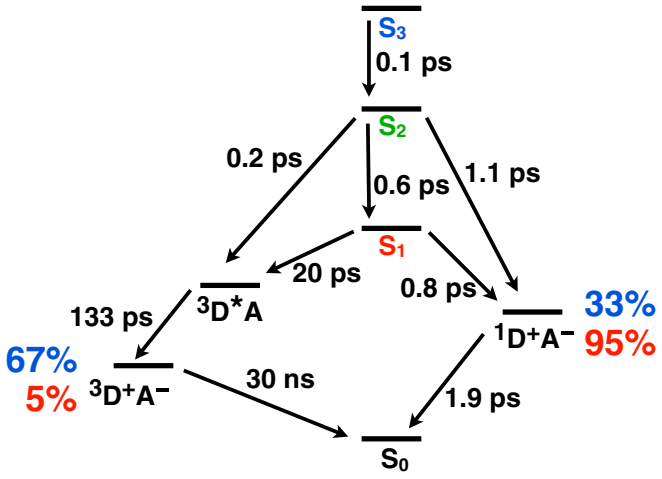

Fig. 6. Kinetics and yields of one-way vs. U-turn ET as a function of excitation wavelength. Time constants are derived from steady-state and time-resolved data. Yields of singlet and triplet ET products upon $S_0 \rightarrow S_3$ (blue) and $S_0 \rightarrow S_1$ (red) excitation are shown as percentages.

The photophysics of RuPZn–NDI sheds light on the ostensibly counterproductive U-turn ET mechanism mustered by the photosynthetic reaction center of *R. sphaeroides*. In the reaction center, ET proceeds from an electronically excited bacteriochlorophyll "special pair" ($^1P^*$, P_MP_L) to a monomeric bacteriochlorophyll acceptor (B_L) exclusively down the L branch (Fig. 7) (19, 20). While fast ET from $^1P^*$ ensures very little intersystem crossing to $^3P^*$, when forward ET is blocked, the triplet yield of *R. sphaeroides* remains essentially zero (21–23). Boxer has shown that S_1 of P_MP_L has a substantial amount of $P_M^-P_L^+$ CT character (24), i.e., $^1P^*$ is polarized away from B_L, toward the M branch. Furthermore, the $^3P^*$ excited triplet state of P_MP_L is delocalized between both bacteriochlorophylls of the special pair, with excess electron density on P_L, i.e., polarized toward B_L (25), underscoring that $^1P^*A$ and $^3P^*A$ of the reaction center are oppositely polarized. We have shown (Figs. 3–5) that singlet and triplet spatial wave functions, sculpted this way, minimize intersystem crossing, safeguarding against $^3P^*A$ formation from $^1P^*A$. The opposite polarization of $^3P^*$ and $^1P^*$ shuts down this intersystem crossing pathway, without impacting the ET rate (*vide infra*) since the transfer mechanism is adiabatic.

Since high-efficiency solar energy conversion devices must operate in the ultrafast kinetic regime, we anticipate that molecular engineering of chromophores that possess oppositely polarized singlet and triplet states may be used to: (*i*) drive high quantum yield formation of charge-separated states, and (*ii*) maximally preserve the energy of the absorbed photon in the resultant charge-separated state (1). Indeed, current state-of-the-art "sensitizers" for dye-sensitized solar cells (2, 26), light absorbers for solar fuel cells (27), and materials for organic photovoltaics (28), suffer from high intersystem crossing yields to low-energy triplet states that limit solar energy conversion efficiency. Asymmetrical supermolecules, such as RuPZn, where molecular design may achieve oppositely polarized singlet and triplet states (Fig. 1 *B* and *C*) that mimic the engineering behind the reaction center special pair, offer an unprecedented level of control over donor intersystem crossing rates, while enabling fast ET events that drive the formation of high-energy, long-lived, charge-separated singlet states. Strongly coupled chromophores that possess internal oxidations and reductions driven by photons of different colors could act as photoswitches to effect desirable photophysical and photochemical processes. Here we have shown RuPZn as an exemplar that links molecular structure to unusual excited-state electronic polarizations that can be used as positive and negative design elements to control ultrafast excited-state dynamics.

Methods

Ultrafast (Femtosecond–Nanosecond) Pump–Probe Transient Absorption Spectroscopy. Ultrafast transient absorption spectra were obtained using standard pump–probe methods (7, 8, 29–32). Following all pump–probe transient absorption experiments, electronic absorption spectra verified that the samples were robust. All reported pump–probe experiments were repeated at least three times with separately prepared samples.

Global Analysis of Pump–Probe Data. Pump–probe transient dynamical data, collected between 410 and 1,100 nm, were globally fit via in-house MATLAB code that accounts for probe chirp (<1 ps) and a Gaussian instrument response. Further details of global fitting can be found in *SI Appendix*.

Time-Resolved Emission. Magic-angle polarization time-resolved emission data were recorded using a Hamamatsu C4780 picosecond fluorescence lifetime measurement system, which utilizes a Hamamatsu Streakscope C4334 photon-counting detector, a Hamamatsu C4792-01 synchronous delay generator, and a Stanford Research Systems DG535 electronic delay generator. RuPZn was excited at 650 nm by the Ti:sapphire laser fed into the optical parametric amplifier of the pump–probe setup described above; the polarization of emission was set to the magic angle (54.7°) for these experiments. Hamamatsu HPD-TA software was used to acquire emission data in the single-photon counting mode, and its fitting module was used to fit the emission lifetime by deconvolution with the experimentally determined instrument response function (irf). The irf was measured using a scattering sample (cream dissolved in water or silica in water). Sample concentrations were adjusted to give an optical density of <0.1 at the excitation wavelength.

Calculation of Quantum Yield Ratios of $^1D^+A^-$ to $^3D^+A^-$. The yield of singlet ET products in RuPZn–NDI upon $S_0 \rightarrow S_1$ excitation was calculated as (1/0.8)/(1/0.8 + 1/20), with 0.8 ps being the ET time constant and 20 ps being the time constant of intersystem crossing. The yield of triplet ET products took 1/20 as

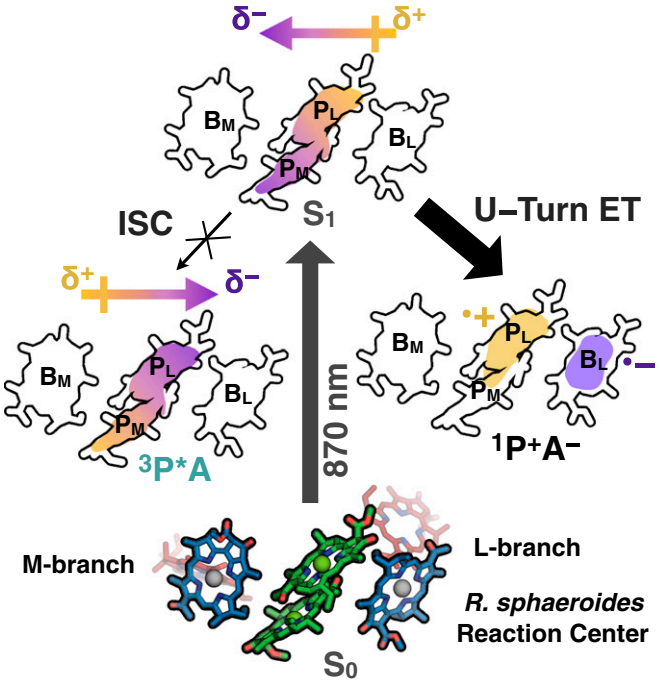

Fig. 7. The bacteriochlorophyll special pair (green, P_LP_M) in the photosynthetic reaction center of *R. sphaeroides* (Protein Data Bank 1AIJ) has oppositely polarized excited singlet and triplet states. The initially prepared singlet excited state undergoes U-turn ET to the monomeric bacteriochlorophyll (blue, B_L) down the L branch to maximize the yield of singlet ET products ($^1D^+A^-$) and avoid formation of the deleterious donor-localized triplet state ($^3P^*A$).

the numerator, as all $^3D^*A$ triplet states proceed to the triplet ET products. To calculate the yield ratio for singlet and triplet ET products of RuPZn–NDI upon S_2 or S_3 excitation, we compared the ratios (R) of the 447 nm (ground-state bleach) transient absorption signal at 250-fs and 10-ps time delay for RuPZn and RuPZn–NDI. Due to the similar, ultrafast timescales of singlet ET in RuPZn–NDI following all excitation conditions, the population remaining at 10-ps time delay is predominately RuPZn-localized $^3D^*A$ states. The yield of singlet ET was calculated as $1 - R_{RuPZn}/R_{RuPZn-NDI}$. The calculated yields of singlet ET for $S_0 \rightarrow S_3$, $S_0 \rightarrow S_2$, and $S_0 \rightarrow S_1$ excitation are 32, 34, and 95%, respectively. The $^1D^+A^-$:$^3D^+A^-$ ratios are then 1:2 ($S_0 \rightarrow S_3$ excitation), 1:2 ($S_0 \rightarrow S_2$ excitation), and 20:1 ($S_0 \rightarrow S_1$ excitation).

Synthetic Materials. All manipulations were performed under argon prepurified by passing through an O_2 scrubbing tower packed with Schweizerhall R3-11 catalyst and a drying tower packed with Linde 3-Å molecular sieves. Air-sensitive solids were weighed in a Braun 150-M glovebox. Standard Schlenk techniques were employed to manipulate air-sensitive solutions. Tetrahydrofuran was purchased from Sigma-Aldrich (inhibitor free, HPLC grade) and all other solvents utilized in synthesis described in this work were purchased from Fisher Scientific (HPLC grade). Triethylamine and acetonitrile were dried over calcium hydride and distilled. All other reagents were used as received (Aldrich or Fisher). Chromatographic purification (silica gel 60, 230–400 mesh, EM Science, and Bio-Beads S-X1, 200–400 mesh, BioRad) of all newly synthesized compounds was accomplished on the benchtop.

ACKNOWLEDGMENTS. N.F.P., T.J., and M.J.T. acknowledge research support from the National Science Foundation through Grant CHE-1709497. D.N.B. acknowledges NIH Grant GM48043.

1. R. E. Blankenship *et al*., Comparing photosynthetic and photovoltaic efficiencies and recognizing the potential for improvement. *Science* **332**, 805–809 (2011).
2. D. Kuciauskas *et al*., Transient absorption spectroscopy of ruthenium and osmium polypyridyl complexes adsorbed onto nanocrystalline TiO_2 photoelectrodes. *J. Phys. Chem. B* **106**, 9347–9358 (2002).
3. N. J. Turro, V. Ramamurthy, J. C. Scaiano, *Modern Molecular Photochemistry of Organic Molecules* (University Science Books, Mill Valley, CA, 2010).
4. S. R. Greenfield, W. A. Svec, D. Gosztola, M. R. Wasielewski, Multistep photochemical charge separation in rod-like molecules based on aromatic imides and diimides. *J. Am. Chem. Soc.* **118**, 6767–6777 (1996).
5. H. Zhu, N. Song, W. Rodríguez-Córdoba, T. Lian, Wave function engineering for efficient extraction of up to nineteen electrons from one CdSe/CdS quasi-type II quantum dot. *J. Am. Chem. Soc.* **134**, 4250–4257 (2012).
6. H. T. Uyeda *et al*., Unusual frequency dispersion effects of the nonlinear optical response in highly conjugated (polypyridyl)metal-(porphinato)zinc(II) chromophores. *J. Am. Chem. Soc.* **124**, 13806–13813 (2002).
7. T. V. Duncan, I. V. Rubtsov, H. T. Uyeda, M. J. Therien, Highly conjugated (polypyridyl) metal-(porphinato)zinc(II) compounds: Long-lived, high oscillator strength, excited-state absorbers having exceptional spectral coverage of the near-infrared. *J. Am. Chem. Soc.* **126**, 9474–9475 (2004).
8. T. V. Duncan, T. Ishizuka, M. J. Therien, Molecular engineering of intensely near-infrared absorbing excited states in highly conjugated oligo(porphinato)zinc-(polypyridyl)metal(II) supermolecules. *J. Am. Chem. Soc.* **129**, 9691–9703 (2007).
9. T. V. Duncan *et al*., Molecular symmetry and solution-phase structure interrogated by hyper-Rayleigh depolarization measurements: Elaborating highly hyperpolarizable D_2-symmetric chromophores. *Angew. Chem. Int. Ed. Engl.* **47**, 2978–2981 (2008).
10. H. C. Fry *et al*., Computational de novo design and characterization of a protein that selectively binds a highly hyperpolarizable a biological chromophore. *J. Am. Chem. Soc.* **135**, 13914–13926 (2013).
11. A. Nayak *et al*., Large hyperpolarizabilities at telecommunication-relevant wavelengths in donor-acceptor-donor nonlinear optical chromophores. *ACS Cent. Sci.* **2**, 954–966 (2016).
12. X. Hu *et al*., Predicting the frequency dispersion of electronic hyperpolarizabilities on the basis of absorption data and Thomas–Kuhn sum rules. *J. Phys. Chem. C* **114**, 2349–2359 (2010).
13. N. P. Redmore, I. V. Rubtsov, M. J. Therien, Synthesis, excited-state dynamics, and reactivity of a directly-linked pyromellitimide-(porphinato)zinc(II) complex. *Inorg. Chem.* **41**, 566–570 (2002).
14. N. P. Redmore, I. V. Rubtsov, M. J. Therien, Synthesis, electronic structure, and electron transfer dynamics of (aryl)ethynyl-bridged donor-acceptor systems. *J. Am. Chem. Soc.* **125**, 8769–8778 (2003).
15. D. Gosztola, M. P. Niemczyk, W. Svec, A. S. Lukas, M. R. Wasielewski, Excited doublet states of electrochemically generated aromatic imide and diimide radical anions. *J. Phys. Chem. A* **104**, 6545–6551 (2000).
16. K. Wynne, R. M. Hochstrasser, "Coherence and adiabaticity in ultrafast electron transfer" in *Advances in Chemical Physics: Electron Transfer-From Isolated Molecules to Biomolecules (Part 2)*, I. Prigogine, S. A. Rice, Eds. (Wiley, New York, 1999), vol. 107, pp. 263–309.
17. G. D. Scholes, G. R. Fleming, A. Olaya-Castro, R. van Grondelle, Lessons from nature about solar light harvesting. *Nat. Chem.* **3**, 763–774 (2011).
18. A. W. Rutherford, A. Osyczka, F. Rappaport, Back-reactions, short-circuits, leaks and other energy wasteful reactions in biological electron transfer: Redox tuning to survive life in O_2. *FEBS Lett.* **586**, 603–616 (2012).
19. B. A. Heller, D. Holten, C. Kirmaier, Control of electron transfer between the L- and M-sides of photosynthetic reaction centers. *Science* **269**, 940–945 (1995).
20. B. Carter, S. G. Boxer, D. Holten, C. Kirmaier, Trapping the $P^+B_L^-$ initial intermediate state of charge separation in photosynthetic reaction centers from *Rhodobacter capsulatus*. *Biochemistry* **48**, 2571–2573 (2009).
21. J. Breton, J. L. Martin, J. C. Lambry, S. J. Robles, D. C. Youvan, *Ground State and Femtosecond Transient Absorption Spectroscopy of a Mutant of Rhodobacter Capsulatus Which Lacks the Initial Electron Acceptor Bacteriopheophytin*, M.-E. Michel-Beyerle, Ed. (Reaction Centers of Photosynthetic Bacteria, Springer Series in Biophysics, Springer, Berlin, 1990), vol. 6, pp. 293–302.
22. M. A. Harris *et al*., Protein influence on charge-asymmetry of the primary donor in photosynthetic bacterial reaction centers containing a heterodimer: Effects on photophysical properties and electron transfer. *J. Phys. Chem. B* **117**, 4028–4041 (2013).
23. C. C. Schenck, W. W. Parson, D. Holten, M. W. Windsor, Transient states in reaction centers containing reduced bacteriopheophytin. *Biochim. Biophys. Acta* **635**, 383–392 (1981).
24. L. J. Moore, H. Zhou, S. G. Boxer, Excited-state electronic asymmetry of the special pair in photosynthetic reaction center mutants: Absorption and Stark spectroscopy. *Biochemistry* **38**, 11949–11960 (1999).
25. S. S. Thamarath *et al*., Electron spin density distribution in the special pair triplet of *Rhodobacter sphaeroides* R26 revealed by magnetic field dependence of the solid-state photo-CIDNP effect. *J. Am. Chem. Soc.* **134**, 5921–5930 (2012).
26. Y. Tachibana, J. E. Moser, M. Grätzel, D. R. Klug, J. R. Durrant, Subpicosecond interfacial charge separation in dye-sensitized nanocrystalline titanium dioxide films. *J. Phys. Chem.* **100**, 20056–20062 (1996).
27. D. L. Ashford *et al*., Molecular chromophore–catalyst assemblies for solar fuel applications. *Chem. Rev.* **115**, 13006–13049 (2015).
28. A. Rao *et al*., The role of spin in the kinetic control of recombination in organic photovoltaics. *Nature* **500**, 435–439 (2013).
29. I. V. Rubtsov, K. Susumu, G. I. Rubtsov, M. J. Therien, Ultrafast singlet excited-state polarization in electronically asymmetric ethyne-bridged bis[(porphinato)zinc(II)] complexes. *J. Am. Chem. Soc.* **125**, 2687–2696 (2003).
30. J. Park, P. Deria, M. J. Therien, Dynamics and transient absorption spectral signatures of the single-wall carbon nanotube electronically excited triplet state. *J. Am. Chem. Soc.* **133**, 17156–17159 (2011).
31. J. Park, P. Deria, J.-H. Olivier, M. J. Therien, Fluence-dependent singlet exciton dynamics in length-sorted chirality-enriched single-walled carbon nanotubes. *Nano Lett.* **14**, 504–511 (2014).
32. J.-H. Olivier *et al*., Near-infrared-to-visible photon upconversion enabled by conjugated porphyrinic sensitizers under low-power noncoherent illumination. *J. Phys. Chem. A* **119**, 5642–5649 (2015).